Tuneable acidity in metal-free mesoporous carbons for hydrolysis reactions

M. Ferri,[a] S. Campisi,[a] P. Carniti,[a] A. Gervasini,[a,*] J. Shen[b]

[a] *Dipartimento di Chimica, Università degli Studi di Milano, via Camillo Golgi 19, 20133 Milano, Italy.*

[b] *Laboratory of Mesoscopic Chemistry, School of Chemistry and Chemical Engineering, Nanjing University, Nanjing 210023, China*

Corresponding author E-mail: antonella.gervasini@unimi.it

ORCID identification numbers of the authors: 0000-0001-6525-7948 (A. Gervasini); 0000-0002-3862-6709 (M. Ferri); 0000-0002-5496-7482 (S. Campisi); 0000-0003-1751-1256 (P. Carniti)

ABSTRACT

A mesoporous carbon (CMC) has been treated under acidic conditions (32.5 wt.% HNO_3 at 10°C or 40°C) to prepare two new carbon samples (HCMC10 and HCMC40), which developed higher acidity in terms of quantity of sites and surface acid strength. The properties of the three carbons have been studied with various techniques (N_2 adsorption/desorption, TEM, XRPD, Raman spectroscopy, ^{13}C NMR, 2D ^{1}H-^{13}C NMR, and XPS). Aromatic –COOH and –OH groups were identified main surface acid sites. Acid site density has been determined by pulse liquid-solid phase adsorption experiments carried out in different liquids. The samples maintained good acidity in water, due to hydrophobicity of the surfaces, while acidity dropped when measured in methanol. From NH_3-TPD analysis, a ranking of acid strength could be obtained: HCMC40 > HCMC10 > CMC. The good acidity of the carbon samples allowed them to act as catalysts in the hydrolysis reaction of sucrose to glucose and fructose. The catalytic activity of the carbon samples was compared with that of Amberlite, a sulfated acid resin; the observed kinetic constant HCMC40 was similar to that of Amberlite.

Keywords: *carbons; porosity; carbocatalysis; surface acidity; acid catalysts; hydrolysis reaction*

1. Introduction

Carbon-based materials include a large variety of structures, from the common activated carbon (AC) and carbon black (CB) to the recent nanostructured carbon allotropes (fullerenes, carbon nanotubes CNTs, carbon nanofibers CNFs, graphene), all playing a central role in heterogeneous catalysis [1]. In particular, carbon materials typically exhibit unique properties as high specific surface areas, tailorable porosities, and high thermal, chemical, and mechanical stability, which justify their wide use as supports for metal-based catalysts.[2] Besides acting as inert supports, carbon materials have been demonstrated to be effective catalysts themselves for several reactions thanks to their functionalized surfaces. This led the way to a new class of carbon-based catalysts representing a metal-free alternative to the more conventional metal and metal oxide catalysts, with enormous benefits in terms of costs, toxicity and durability.[3–10] Remarkable performances of carbon-based metal-free catalysts have been reported for many reactions of industrial interest, such as oxidative and direct dehydrogenation,[11,12] oxygen evolution reaction (OER),[11] liquid-phase oxidation of hydrocarbons,[11,13–17] oxygen reduction reaction (ORR),[11,18,19] hydrogen evolution reaction (HER),[11,20] hydrogenation,[11,21–23] Friedel–Crafts reactions,[11,24–26] Michael addition,[11,27] and aldol condensation[11,28]. Recently, metal-free carbon-based catalysts have been successfully used also in chemical transformations for biomass valorization.[29–34]

Two key aspects should be taken into account in the development of metal-free carbon catalysts with high efficiency and long durability: the control of porosity and the identification and design of the active sites. Actually, a fine regulation of porosity can have a positive impact both on mass transfer phenomena and on the exposure of active sites. From this point view, ordered mesoporous carbons (OMC)[35,36] as well as hierarchically porous carbon materials[37–39] represent two examples of interesting structures with optimized porosity which are receiving great attention for their application in catalysis. On the other hand, tailoring the nature and structure of active sites is

fundamental, especially when liquid phase reactions with complex pathways are involved, as in the case of biomass transformations.

Surface functionalization of carbon materials results in the introduction of heteroatoms (e.g. oxygen, nitrogen, boron, sulfur, and phosphorus), which modify the electronic properties, the hydrophilicity and the surface acidity of the carbon materials.[40,41] Wet chemical methods are traditionally used for the chemical modification of carbon materials at the surface. Mineral acids (HNO_3, H_2SO_4, H_3PO_4 and HCl) or strong oxidant agents (H_2O_2, $KMnO_4$) are widely employed for this purpose [42,43]. However, the imposed harsh operative conditions often lead to pore collapse and morphology modifications of carbon materials. Consequently, the main challenge lies in the ability to conjugate the control of porosity with a limited surface modification of carbon structures.

In this work, a wheat flour derived mesoporous carbon (CMC) already presented in the literature, [44] has been functionalized by treatment with HNO_3 under mild conditions (up to 40°C) in order to preserve the mesoporosity and the structure of the pristine material. Particular attention has been devoted to the determination of the surface properties by a combination of different characterization techniques (N_2 adsorption/desorption, XRPD, Raman spectroscopy, ^{1}H and ^{13}C NMR, XPS, and acidity measurements). The obtained materials have been tested in the acid-catalyzed hydrolysis of a simple disaccharide to prove their effectiveness as acid catalysts and useful structure-activity relationships.

2. Experimental section

2.1. Materials

CMC was prepared as reported in Ref.[44]. 1:1 diluted HNO_3 from 65% m/m (Fluka) was used as oxidizing agent to obtain the functionalized HCMC10 and HCMC40 samples. 2-phenylethylamine (PEA, >99.0%, from Sigma-Aldrich) and benzoic acid (BA, >99.0%, from Carlo Erba) were used for solid-liquid acid and base titrations, respectively. Cyclohexane (>99.5%, GC grade), methanol

(>99.9%, HPLC grade) and water (HPLC grade), purchased from Sigma-Aldrich, were used as liquids for acid/base titrations and for preparing the PEA and BA solutions. Powder sea sand (Fluka, acid-purified) and silanized glass wool (Sigma-Aldrich) were used as inert materials during column filling.

For gases, N_2 (99.9995% purity) and NH_3/N_2 (1% v/v) from SAPIO were employed. Amberlite IR120(H) resin (Carlo Erba) was used as reference acid catalyst and used in the acidic titrations and catalytic tests. The resin was washed and activated before use following the recommendation of the producer. Sucrose (pure reagent, Carlo Erba) solution (in HPLC grade water) was used as reagent in the hydrolysis catalytic tests. Ca-EDTA dihydrate (pure reagent, Titriplex) 0.005 M solution in HPLC grade water (as mobile phase in HPLC analyses were used) and D-Glucose/D-Fructose enzymatic kit purchased from r-Biopharm (Boehringer Mannheim, Roche) were used for the determination and quantification of sucrose hydrolysis reaction products.

2.2. Synthesis of CMC

The preparation of CMC was performed as follows, wheat flour and $ZnCl_2$ were mixed in water and then treated at 85°C for 3 h until a dark brown paste was obtained. The paste was treated at 130°C for 1 h under air, yielding a black solid. Carbonization was then accomplished by thermal treatment (450°C for 2 h) under inert atmosphere (nitrogen flux). The material was finally washed with 1 M HCl and boiling water until neutrality, to eliminate the residual $ZnCl_2$, and finally dried at 130°C for 6 h.

2.3. Acidic functionalization of CMC

Acidic functionalization was carried out at 10°C (HCMC10) and 40°C (HCMC40). In a typical functionalization procedure, ca. 10 g of CMC were put in contact with 150 mL of HNO_3 32.5wt.% in a jacked reactor for 17 h at constant temperature. The solids were then filtered, rinsed with distilled water until neutrality of the filtrate and then dried at 120°C under air for 8 h.

2.4. Characterization

N_2 adsorption-desorption isotherms were obtained at liquid nitrogen temperature, using a Sorptomatic 1990 version instrument from Thermo Scientific (Carlo Erba). The analysis was controlled by computer processing using the MILES-200 program and the MILEADP software for computations. The low-pressure part of the adsorption branch of the isotherm ($0.03 < p/p^0 < 0.35$) has been modeled by the BET equation for the determination of specific surface area. The desorption branch has been elaborated by B.J.H. model (Barrett-Joyner-Halenda) for pore size and pore size distribution determination. Prior to the analysis, ca. 0.1 g of dried sample were outgassed for 4 h at 150 °C under a residual pressure of 0.1 mbar in order to free the pores from residual water. The adsorbed volume, expressed in $cm^3(STP)\cdot g^{-1}$, was converted into pore volume, $cm^3\cdot g^{-1}$, using the density of N_2 in the normal liquid state (ρ=0.8081 g cm g^{-1}); molecular area of N_2 was taken as 16.2 Å.

Electron scanning microscopy with energy dispersive X-rays (SEM-EDX) mapping were carried out on pristine CMC samples using a Leo Zeiss microscope equipped with EDX probe. Operational parameters were set as follows: chamber pressure equal to $9\cdot10^{-7}$ torr, electron gun current = 3.58 A and applied voltage of 20 kV.

Transmission electron microscopy (TEM) was carried out on an EFTEM Leo912 ab (Zeiss, Oberkochen, Germany) at 100 kV under vacuum with tungsten filament source. A weighted amount of sample powder (*ca*. 5-7 mg) was dispersed in isopropanol and sonicated for 15 minutes. To improve sample homogenization, the suspension was further mixed in a vortex mixer (ca. 10 s) and finally diluted (0.01 mL in 1 mL). A 10 µL aliquot of the diluted suspension was adsorbed on 300 mesh formvar/carbon copper grids (Cu 300 FC). The grids were dried at r.t. overnight before observation.

X-ray powder diffraction analyses (XRPD) were performed on CMC, HCMC10 and HCMC40 samples using a Philips Powder X-ray diffractometer equipped with a PW 1830 generator.

Monochromator was made in graphite, operating with Cu Kα (λ = 1.5418 Å) radiation. The X-ray tube worked at 40 kV×40 mA. The acquisition range 2θ range of the diffraction patterns was from 10° to 70°. Scan rate was fixed at 0.6° min−1 with a step size of 0.05°.

Raman spectroscopic analyses were conducted using a Raman Jasco RMP 100 microprobe, coupled with a Lotoriel MS 125 spectrophotometer with a ND-YAG laser (λ = 532 nm) as light source.

^{1}H and ^{13}C NMR spectra were collected using an NMR Spectrometer AvanceTM 50 equipped with a 4 mm MAS probe for direct acquisition from solid samples; spectra were registered at 35°C at an optimized resonance frequency of 125.77 MHz. All samples were mixed with ZrO_2 prior to analysis and place in Kel-F sealed NMR tubes (internal volume = 50 μL).

Surface acidic/basic sites were titrated in liquid phase in liquids with different polarity-proticity (cyclohexane, water and methanol) using a modified HPLC line, constituted by a L-6200 A Merck Hitachi pump, a AS-2000A Merck Hitachi autosampler and a UV-Visible L-4250 Merck Hitachi detector operating at 254 nm (paragraph S.1., Fig. S.1.1). At first, a sample mass of ca. 20 mg was crushed, sieved as 80-200 mesh particles, and then placed in a sample holder (stainless steel tube, 2 mm diameter and 10-12 cm of length) between two sand pillows. It was then thermally activated (7 mL min^{-1} under air flowing for 3 h at 150°C) and successively vacuum-wetted with the appropriate liquid. The filled sample holder was then put at the place of the chromatographic column (L-5025 Merck column thermostat at 25°C). Analysis was carried out with liquid flow rate of 5 mL min-1 and injections of fixed volume of probe solution were regularly made (Δt_{inj} = 5 min, 20 μL of PEA at ca. 0.12 M and or 20 μL of BA at ca. 0.05M, in cyclohexane, and ca. 0.025M, in water and methanol). A chromatogram constituted by successive increasing peaks was obtained (Fig. S.1.2) Saturation was considered to be reached when, for successive titrations, constant peaks' height and area were obtained. The numerical interpretation of the collected data was performed as reported elsewhere [45], all details are reported in paragraph S.1.

Thermo-desorption analysis of ammonia (NH_3-TPD) was carried out from NH_3-saturated samples by operating in a home-made adsorption/desorption line. The line was equipped with a set of mass flow controllers (Bronkhorst, Hi-Tec and Brooks Instruments), a tubular vertical electric oven (Eurotherm controller-programmer type 818), a quartz tubular sample-holder with porous septum (5 mm i.d.) for placing the sample (*ca*. 0.05 g, 80-200 mesh particle size) and coupled with a FT-IR spectrophotometer (Bio-Rad, DTGS detector). The saturation was performed on thermally activated samples (120°C for 30 min under N_2 flowing (50 ml·min^{-1}) monitoring the adsorbed and desorbed NH_3, following continuously the line at 926 cm^{-1} (N-H asymmetric stretching, wagging mode) as a function of temperature. After attainment of saturation, at first, an isothermal step at 150°C was performed to remove the excess of adsorbed ammonia from the surface (physisorbed) until stable signal was obtained. Then, temperature was raised at 10°C·min^{-1} to 800°C. Fig. S.1.3 reports the whole operative procedure. Assuming a 1:1 stoichiometry for adsorbed ammonia on the acid site, the total number of sites could be known and expressed as equivalent of acid site per sample unit mass or unit surface (mequiv·g^{-1} or mequiv·m^{-2}).

X-Ray photoelectron spectroscopy was employed to investigate the surface composition of the samples. The analyses were carried out on a M-PROBE Surface Spectrometer, using an Al (K_α) source and a spot size from 0.15 mm to 1 mm in diameter. The voltage was 10 V and the vacuum 10^{-7} -10^{-8} Torr. The survey scans were carried out in the binding energy range 0-1100 eV, using a spot size of 800 micron. The energy resolution was 4 eV and the scan 1 eV/step. The software used for data analysis was ESCA Hawk Software.

2.5. Catalytic tests

The ability of CMC, HCMC10 and HCMC40 samples in catalyzing sucrose hydrolysis was tested in an Atlas Syrris Batch Slurry reactor (USA), in aqueous solution. Ca. 1 g of dried catalyst was dispersed in 150 mL of a 50 mM sucrose solution; reaction temperature was set at 80°C under

gently magnetic stirring. Kinetics of sucrose hydrolysis was monitored by reaction mixture withdrawals (1 mL for HPLC analyses, 100 μL for enzymatic kit analyses) at fixed time up to ca. 24 h.

Analyses of the products of sucrose hydrolysis were carried out using an HPLC line constituted by a Waters 515 HPLC pump, a 717 Plus Waters autosampler, a SugarPak column (operating at 90°C in a column thermostat) and a Waters 410 Differential Refractometer as detector (cell temperature = 40°C). The mobile phase was a 10^{-4} M Ca-EDTA aqueous solution and the samples injected volume was 20 μL. After peaks integration, the concentration of eluted compounds was evaluated in terms of concentration of monosaccharides units. Analyses of reducing sugars were performed with a r-Biopharm D-Glucose/D-Fructose enzymatic kit according to the producer's recommendation.

As sucrose hydrolysis is a well-known first order reaction [46], the reaction rate can then be mathematically described as:

$$\nu = k_{obs} \cdot [sucrose]$$

The observed kinetic constant, k_{obs}, contains the catalyst concentration, [*catalyst*], and the catalytic constant, k_{cat}:

$$k_{obs} = k_{cat} \cdot [catalyst]$$

it is possible to express [*catalyst*] in $g \cdot L^{-1}$ or in $m^2 \cdot L^{-1}$. Then, k_{cat} is expressed in $L \cdot g^{-1} \cdot t^{-1}$ or in $L \cdot m^{-2} \cdot t^{-1}$, respectively.

3. Results and discussion

3.1. Composition, morphology and structure of carbon samples

CMC is a mesoporous carbon material provided by the research group of Shen et al.[44] through an innovative synthetic procedure. The material develops mesoporosity and higher purity compared to conventional activated carbon.

The content of impurities was estimated to be < 1% by SEM-EDX chemical analysis, thus confirming the high purity of CMC (Fig. 1, a). The most of impurities are Cl, Zn and Fe, deriving from the synthetic route. In addition, the low content of oxygen (6.34%) indicates that CMC is not highly functionalized in comparison with activated carbons.

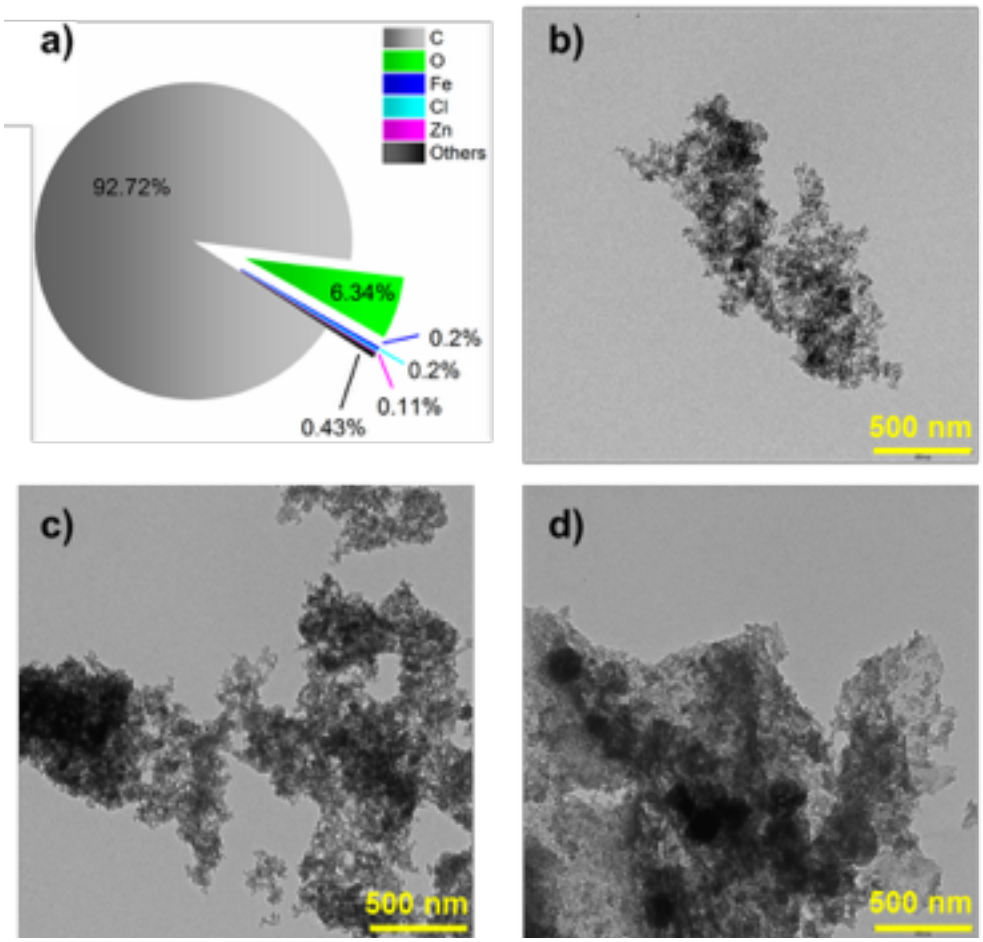

Fig. 1. Percent composition of a) CMC sample from SEM-EDX analysis and TEM images of b) CMC, c); HCMC10 and d) HCMC40 at same magnification.

In order to introduce surface acid functionalities on CMC, acid treatments were carried out. Mild conditions (HNO_3, 32.5wt.%, at 10°C for HCMC10 or at 40°C for HCMC40) were adopted to preserve the mesoporosity of the CMC, since too harsh functionalization conditions are supposed to negatively impact on the carbonaceous framework and porosity.

TEM micrographs revealed that all carbon samples presented similar morphology, characterized by a disordered porous structure, in particular HCMC40 (Fig. 1, b-d).

The surface area and porosity of pristine CMC sample and the functionalized HCMC10 and HCMC40 samples were investigated by N_2 adsorption/desorption isotherms (Fig. 2).

CMC sample confirmed to be a mesoporous material exhibiting high surface area (ca. 1465 $m^2 g^{-1}$), as previously reported by Shen et al.[44] After the acidic functionalization treatment, surface area values of HCMC10 and HCMC40 decreased, as expected, the latter sample possessing surface area value reduced by approximately 40% compared to CMC (Table 1). Concerning porosity, the mesoporous feature of CMC was preserved in HCMC10, while some microporosity appeared in the HCMC40 sample (Fig. 2); the appearance of microporores in HCMC40 was associated with a negative C_{BET} constant. Accordingly, the pore volume value of HCMC10 has almost halved compared to CMC and a more remarkable decrease was observed for the HCMC40 sample (Table 1).

A closer inspection of the collected N_2 adsorption/desorption isotherms indicated that a slight change in mesoporosity between CMC and HCMC10 occurred, as the latter sample had mesopores centered at value lower than 20 Å of pore radius.

Table 1. Morphological results of the three carbon-samples determined by N_2 adsorption-desorption experiments.

Sample	C_{BET} [a]	Surface area $m^2 \cdot g^{-1}$	Pore volume $cm^3 \cdot g^{-1}$	PSD Å
CMC	125	1465	2.5	23.8
HCMC10	229	1143	1.4	19.6
HCMC40	-113	845	0.8	18.4

[a] obtained from two parameter BET equation.

The observed modifications in surface area and porosity could be associated also to eventual changes in the structure of the carbon frameworks. Structural characterization was then performed to assess the effect of acid treatment on the carbon skeleton. XRPD patterns and Raman spectra for CMC and acid-treated samples, HCMC10 and HCMC40, are reported in Figure 3, respectively. The only important features in the XRPD patterns are two broad and weak diffraction peaks at 2θ angles centered between 20°-30° and between 40°-50°, which can be indexed as 002 and 10 reflection lines and are typical of amorphous carbon materials composed of small random stacked hexagonal aromatic sheets.[47,48] The broadening of the 002 reflection peaks as well as the shift towards lower angles indicated a decrease in the dimensions of graphitic domains and in the order of crystallinity of the two carbon materials treated in acid (25°2θ for CMC to *ca*. 23°2θ for HCMC10 and HCMC40).

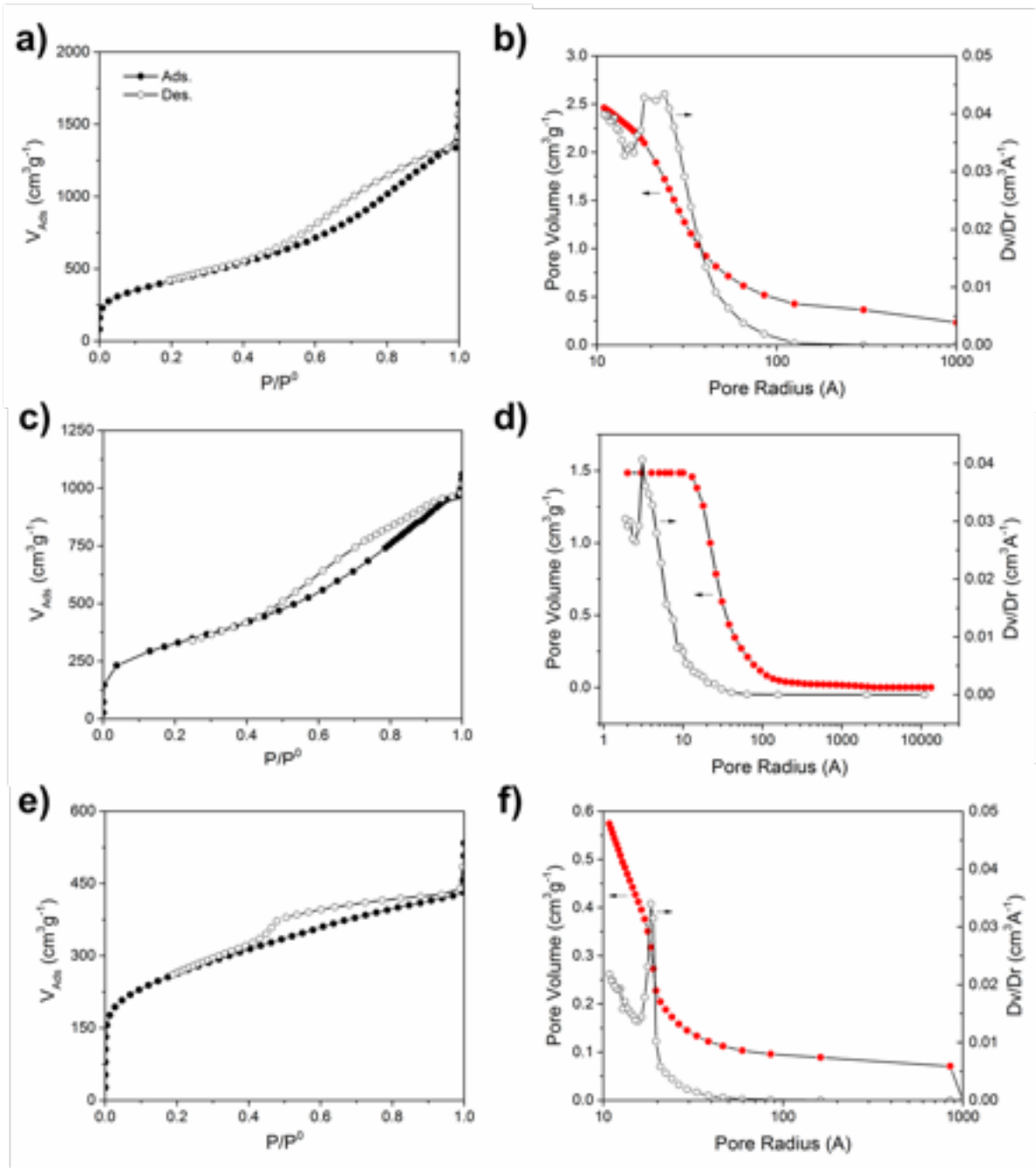

Fig. 2: Morphological results of the three carbon samples determined by N_2 adsorption-desorption experiments at -196°C (a, c, e) and relevant pore size distribution (b, d, f) obtained by BJH model equation on CMC (a, b); HCMC10 (c, d); and HCMC40 (e, f).

The Raman spectra were dominated by two bands typical of carbon materials: the so called G band (1530-1620 cm^{-1}), associated to the graphite in-plane E_{2g} Raman active mode, and the disorder-related D band (A_{1g} D breathing mode)[49] at ca. 1350 cm^{-1}. The intensity ratio of the D band to the G band (I_D/I_G), which is usually considered as an index of the disorder and defect

concentration, was *ca*. 0.8 for all the three materials, indicating in any case the presence of graphitic domains with average size of *ca*. 1 nm.[50]. A focus on peak positions revealed that the acid treatment of CMC produced a downshift in the position of the G peak (from 1613 cm^{-1} for CMC to 1600 cm^{-1} for HCMC40). This behavior has been reported to originate from competing factors, including both an increase in bond disorder and in the amount of sp^3 carbon.[51] However, the cause of the shift is often more complex, and other effects, such as strain and electronic interactions, could be also taken into account.

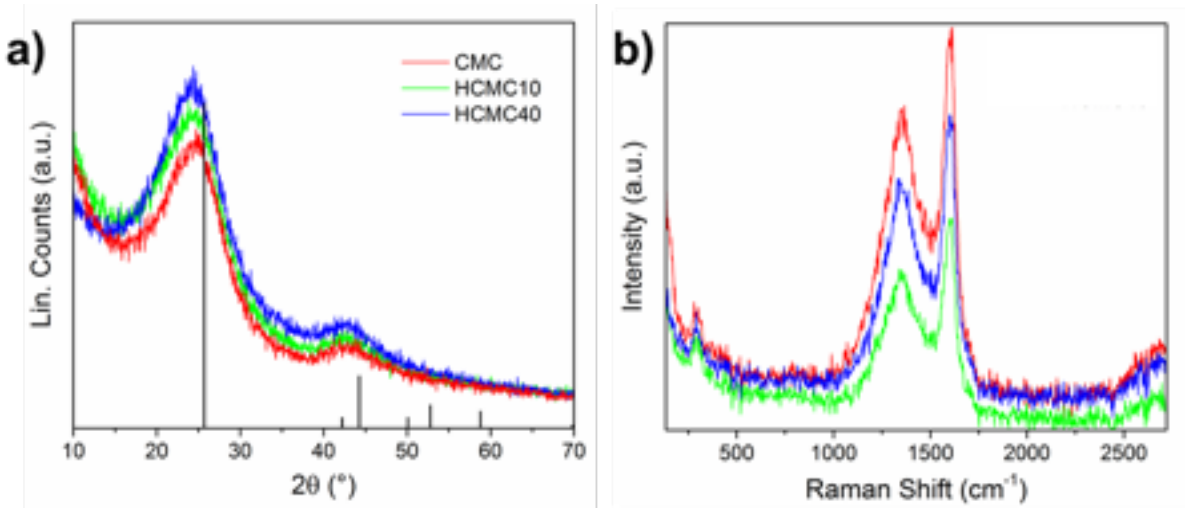

Fig 3. Structural characterization results of the three carbon samples: a) XRP-Diffraction and b) Raman spectroscopy.

The information provided by morphological and structural characterization supported the idea that acid functionalization of CMC led to the breaking of graphitic domains with an increase of edge sites terminating with oxygen functionalities (e.g. carboxylic acids, lactol, hydroxyl and carbonyl groups).

To disclose the nature of the O-functionalities in the HCMC10 and HMC40 samples, solid state ^{13}C-NMR spectra were collected (Fig.4). ^{13}C-NMR spectra of all the three samples were characterized by an intense signal at chemical shift of *ca*. 127 ppm, assigned to highly condensed polyaromatic hydrocarbons. Additional features at 165 and 185 ppm, typical of hydroxyl groups and

carboxylic acids, were also present and became more intense in HCMC10 and HCMC40. The 2D $^{1}H-^{13}C$ HETCOR CP-MAS NMR spectra (paragraph S.2., Fig. S.2.) revealed correlations exclusively between protons at *ca*. 7 ppm and carbon atoms at 127 ppm, thus confirming that only aromatic moieties are present in all the three carbon samples.

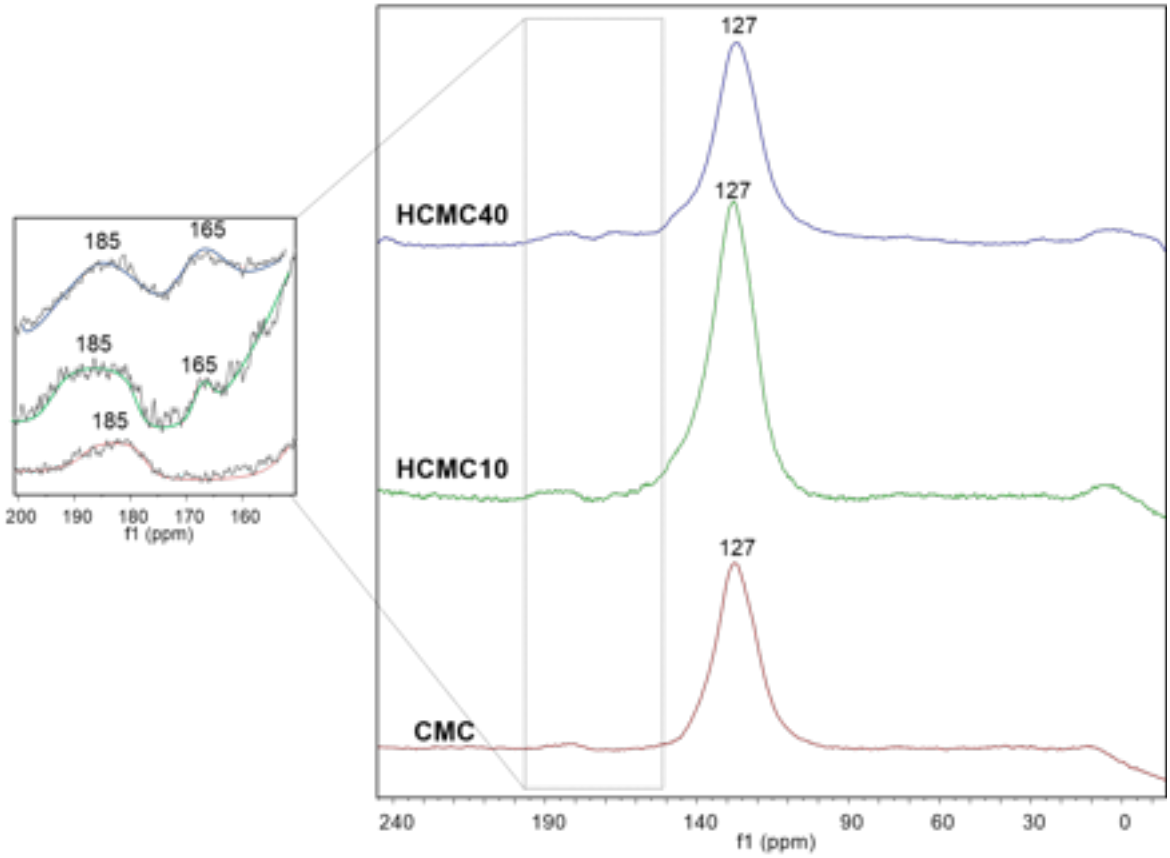

Fig. 4. Nuclear Magnetic Resonance results of the three carbon samples: ^{13}C NMR spectra, with a magnification in the 200-150 f1 zone.

3.2. Surface properties of carbon samples

3.2.1. Surface composition.

The surface modification induced by acid treatments of CMC was investigated by X-ray photoemission spectroscopy (XPS), which provided useful insight on the nature and amount of species at the surface (Fig. 5). The survey XPS scans were dominated by C 1s and O 1s peaks (N, Si and Cl, being additionally present as impurities). The area of O 1s peak increased going from CMC

to HCMC10 and HCMC40, confirming the successful introduction of oxygen functional groups at the carbon surfaces by acid treatment. In particular, the oxygen content was calculated to be 7.4 at. % in CMC, 10.8 at.% in HCMC10 and almost doubled (13.6 at.%) in HCMC40 (Fig. 5, b). The focus on C 1s and O 1s regions revealed interesting details on the nature of oxygenated groups introduced after functionalization. The C 1s and O 1s high resolution regions are reported in Fig. 5, c and 5, d. Curves' deconvolution enlightened clear differences of the surface species between pristine CMC and HCMC10 and HCMC40.

All C 1s XP spectra were deconvoluted into a sp^2-hybridized carbon C=C (*ca*. 284.5 eV), a sp^3-hybridized carbon C–C/C– H (*ca*. 285.6 eV) and the additional peaks associated with oxygen functional groups (Fig. 5, c). The relative percentage of these components strongly differs from sample to sample. In particular, at the HCMC10 and HCMC40 surface, the acid and oxidative treatment affected the graphitic carbon structure, producing a defective structure rich in oxygen functionalities, as corroborated by the decrease of sp^2-hybridized carbon and concomitant increase of sp^3-hybridized carbon compared to CMC. Concurrently, the contribution of components related to oxygenated species (C–O. C– O– C, C=O, OC=O) became more relevant in HCMC10 and HCMC40. Additionally, interesting differences emerged between HCMC10 and HCMC40 samples concerning the nature of oxygenated species. Indeed, acid treatment at low temperature (HCMC10) seemed to favour the introduction of ether and hydroxyl groups (C–O, C–O–C, 286.6-286.9 eV), while carboxyl groups (288.8-290.4 eV) were predominant in HCMC40. These differences appeared more evident in the deconvoluted O 1s XP spectra (Fig. 5, d). The deconvolution of the O 1s spectra for CMC showed the following four components: i) ketonic carbonyl oxygen band (531.0–531.9 eV), ii) carbonyl oxygen atoms in esters, anhydrides, and oxygen atoms in hydroxyl groups (532.3–532.8 eV), iii) non-carbonyl (ether-type) oxygen atoms in esters and anhydrides (533.1–533.8 eV) and iv) adsorbed water and/or oxygen (536.0–536.5 eV). The deconvoluted O 1s

spectra of HCMC10 and HCMC40 presented an additional component in the region 534.3–535.4 eV, typical of oxygen atoms in carboxyl groups. This component was more intense and complex in the case of HCMC40, whereas the predominant contribution in HCMC10 derived from carbonyl and hydroxyl groups. This evidence confirmed that the temperature of acid treatment could tune the nature of oxygenated species formed on carbon surfaces: the higher the temperature, the higher the amount of carboxylic functionalities.

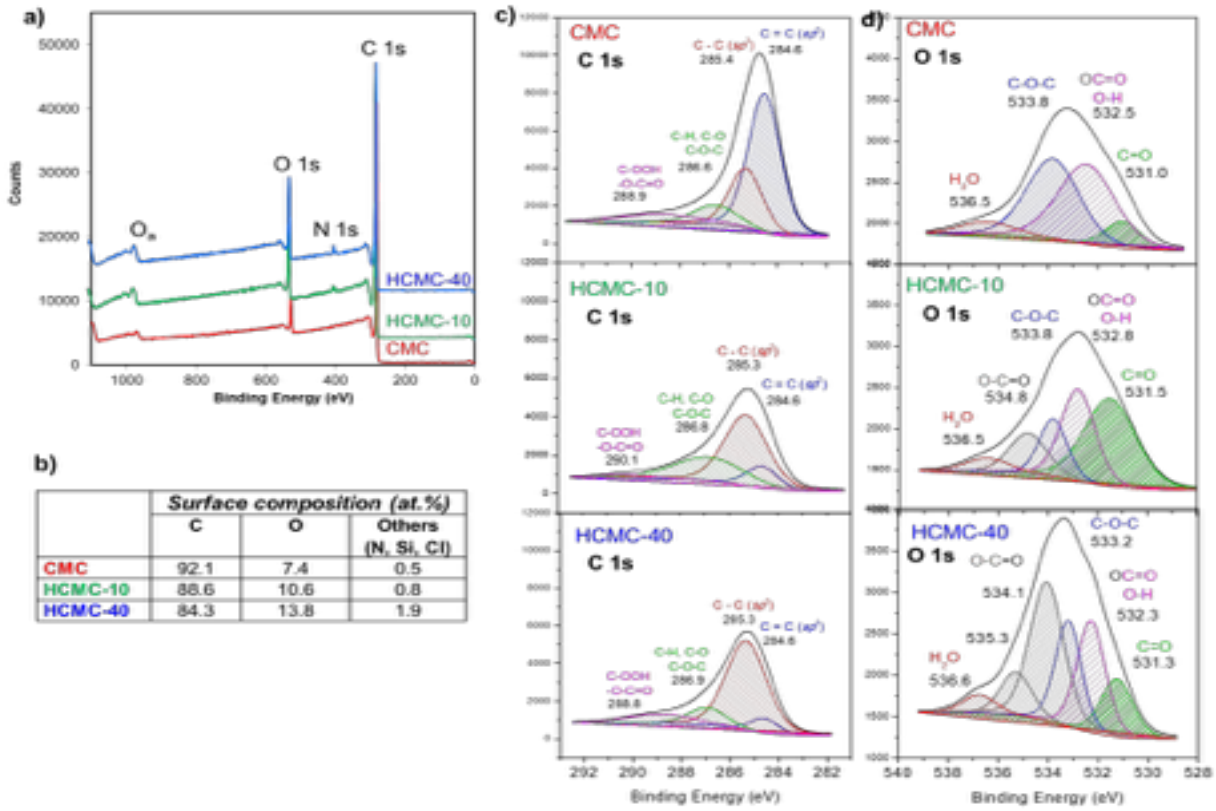

b)

	Surface composition (at.%)		
	C	O	Others (N, Si, Cl)
CMC	92.1	7.4	0.5
HCMC-10	88.6	10.6	0.8
HCMC-40	84.3	13.8	1.9

Fig. 5. Surface composition analysis by XPS of the three carbon samples: a) survey scan; b) percent surface composition; c) high-resolution C 1s: d) high-resolution O 1s spectra.

3.2.2. Surface acidity.

The presence of carboxylic and other oxygen-containing groups at the surface of HCMC10 and HCMC40 was expected to increase the acidity of the surfaces. The number of acid sites of the CMC, HCMC10 and HCMC40 surfaces was evaluated by means of pulse liquid-solid phase titrations in different liquids, using phenylethylamine (PEA) as probe molecule. Moreover, surface basicity of the pristine CMC sample was determined in different liquids, using benzoic acid (BA) as probe molecule (Fig. S.1.4).

Titrations were performed in three different liquids, namely cyclohexane, water, and methanol. Being an aprotic and non-polar solvent, cyclohexane does not compete with the used probe molecules (PEA and BA) for the interaction with the surface acid/basic groups, thus allowing the evaluation of the *intrinsic* acidity of the materials. On the other hand, since the samples were tested in catalytic hydrolysis reactions in water (see 3.3 paragraph), titrations in polar protic solvents are fundamental to assess if the sample surfaces retained their acidic features under working conditions (*effective* acidity). All the collected titration results are reported in Fig. 6 and the numerical data are reported in Table S.1.1.

Intrinsic acidity of the samples, determined in cyclohexane, increased in the order CMC<HCMC10<HCMC40 (Fig. 6, a). The increase of acidity was observed both in terms of concentration (meq g^{-1}) and density (μeq m^{-2}) of acidic sites (Table S1). All the samples resulted to retain their acidic feature in aqueous environment (Fig. 6, b), the *effective* acidity in water followed the same above-reported trend. In water, only a very slight decrease of the total number of acid sites was detected for the three carbon samples (Table S1), confirming the water-tolerant nature of the surface acid sites, probably due to hydrophobicity of the carbonaceous structure, which did not suffer the water adsorption.

When titrated in methanol, the surface acid sites of the three samples resulted drastically reduced, down to ca. one fourth of the total sites determined in cyclohexane and/or in water (Fig. 6, c and Table S.1.1). The higher lipophilicity of methanol, likely, allowed a more intimate contact with the carbon surface, so masking some acid groups of the surface.

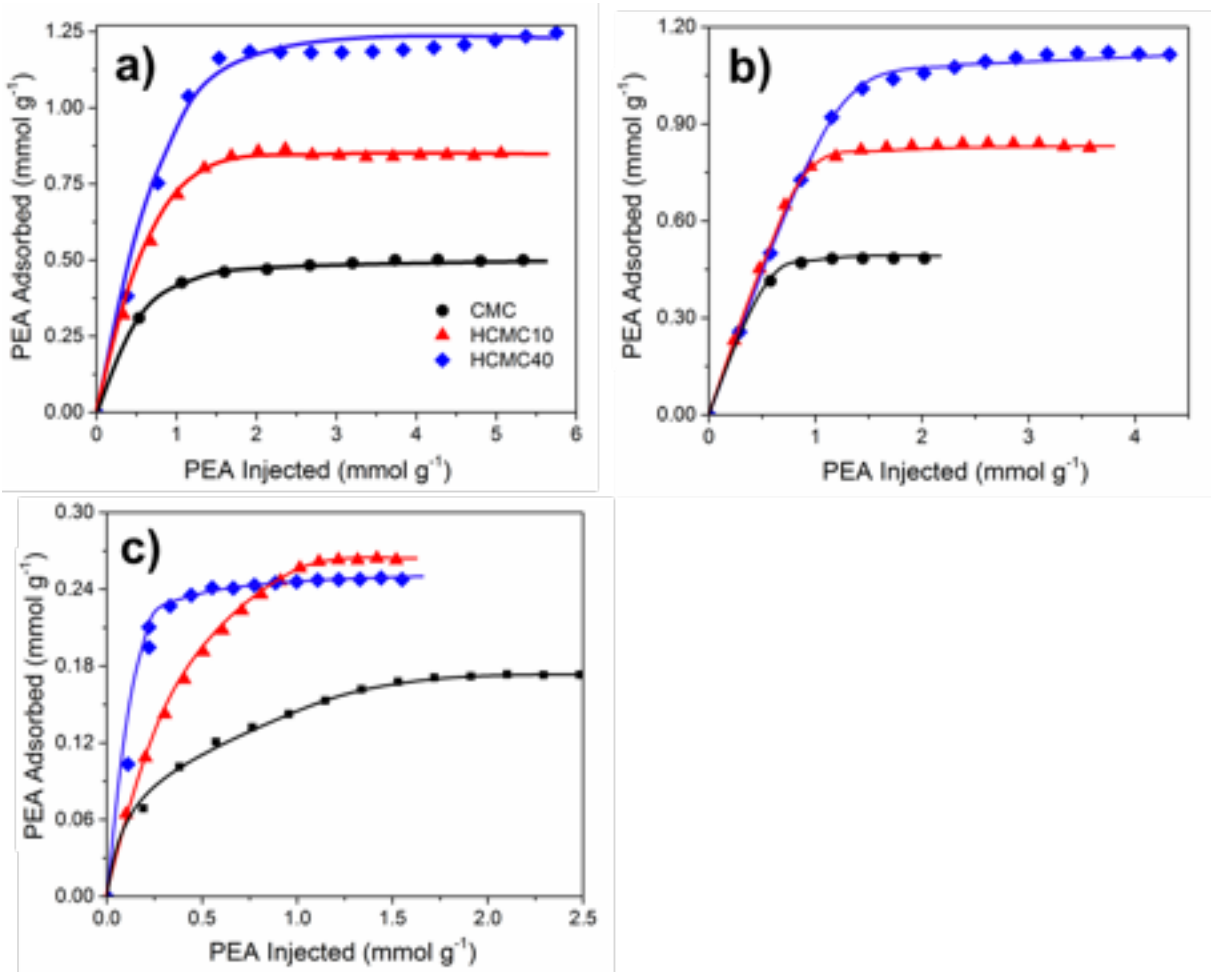

Fig. 6. Acidity results of the three carbon samples obtained from the pulse liquid phase adsorption experiments with PEA in three different liquids: a) cyclohexane; b) water; and c) methanol.

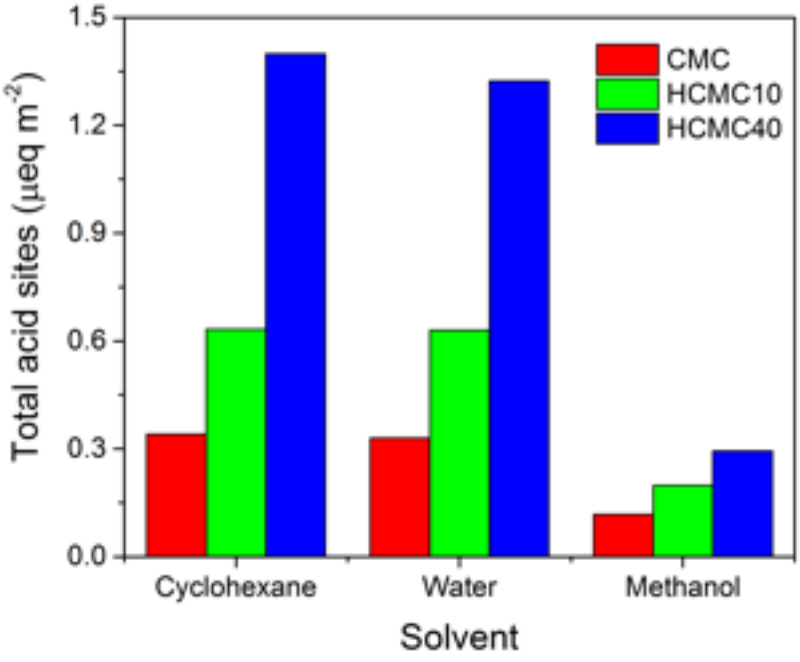

Fig. 7. Comparative results of acidity titrations on CMC (red), HCMC10 (green) and HCMC40 (blue) determined with PEA probe by pulse liquid phase adsorption experiments in three different liquids: cyclohexane (*intrinsic* acidity), water and methanol (*effective* acidity).

A comparative final view on the titration results is shown in Fig. 7, where the results in terms of *intrinsic* (cyclohexane) and *effective* (water and methanol) acid sites are reported; the very low *effective* acidity of the three samples in methanol is well evident.

CMC possessed also a very moderate intrinsic basicity (Table S.1.1), as emerged from titrations with benzoic acid in cyclohexane (the number of basic sites was a quarter of the acid sites). According to the literature,[52] the basicity of carbon surfaces could derive both from basic oxygen groups, associated with chromene-, pyrone- and quinone-type moieties, and from Lewis type groups, ascribable to π electron-rich regions on the basal planes of the graphitic domains.

NH_3-TPD analyses were performed with the aim of studying the surface acid strength of the three carbon samples; the presence on HCMC10 and HCMC40 of several oxygenated groups formed by acid-treatment of CMC could also be associated with an increase of acid strength of the samples.

The NH_3-TPD profiles of CMC, HCMC10 and HCMC40, reported in Fig. 8, evidence that all carbon samples possess acid sites of medium acid strength (low temperature band in the 250-400°C range), whose amount linearly increase going from CMC to HCMC10 and HCMC40. Only in the case of HCMC40, an additional desorption band was present at high temperature (550-800°C interval) . This band might reveal a population of strong acid sites, likely associated with carboxylic groups, which are present only in HCMC40, as suggested by XPS. The total amount of NH_3 desorbed almost doubled going from CMC to HCMC10 and to HCMC40, as already found for PEA titrations in cyclohexane (Table S.1.1.). This observation agrees also with the amount of NH_3 adsorbed by the three samples during the saturation step of the NH_3-TPD procedure (Fig. S.1.3). In summary, from NH_3-TPD analyses, it emerged that the number of acid sites and the acid strength are incremented by the oxidative and acid treatment,with the possibility to tune acidity act on treatment's condition.

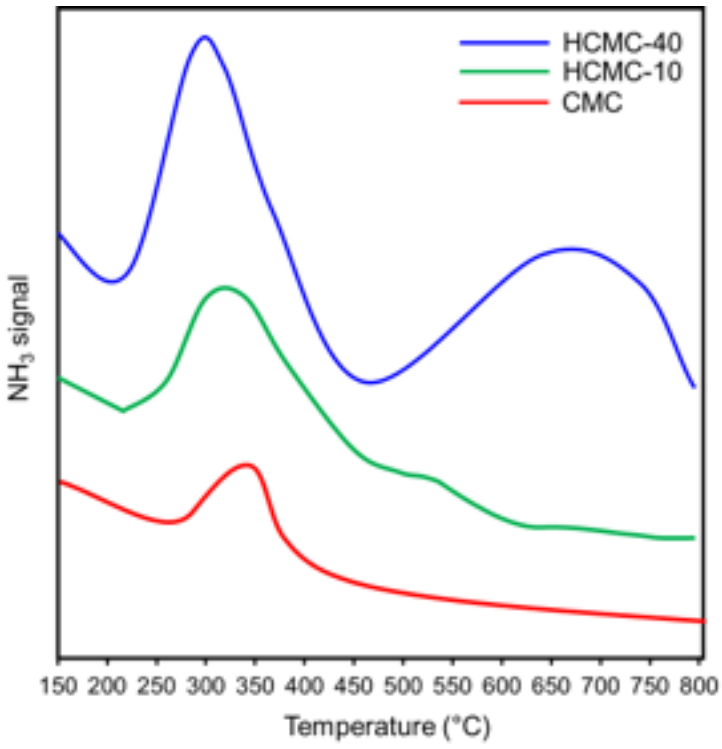

Fig. 8 NH_3-TPD profiles of CMC, HCMC10 and HCMC40 materials

3.3. Test reaction of catalytic sucrose hydrolysis

Pristine CMC and acid-treated HCMC10 and HCMC40 samples have been tested as solid acid catalysts in the reaction of sucrose hydrolysis to evaluate their effective ability to cleave the glycosidic α–β 1-2 bond of sucrose. The catalytic performances of the carbon samples have been compared to an industrial benchmark catalyst such as Amberlite IR-120(H), which is a well-known acid resin. Sucrose hydrolysis tests have been performed in a batch reactor under mild conditions (80°C, atmospheric pressure, in water as the solvent), with a fixed catalyst concentration of 0.0067 g mL^{-1}.

Catalytic results are represented in Fig. 9, where the residual concentration of sucrose and the corresponding concentrations of products (glucose and fructose) are plotted as a function of reaction time. All the results collected during catalytic tests are also available as numeric data in paragraph S.3., Tables S.3.1 to S.3.4. Under the operative conditions, as expected, all catalysts demonstrated to be able to selectively break the glycosidic bond of sucrose, producing glucose and fructose. No other products have been detected by HPLC analyses. The high selectivity of the hydrolysis reaction was further confirmed by the mass balance expressed in terms of concentration of mono-saccharide equivalents (Tables S.3.1 to S.3.4), which resulted to be constant at every sampling time. In addition, in every case, the concentration profiles of fructose and glucose were perfectly overlapped (Fig. 9, a-c-e-g). The 1:1 stoichiometry of hydrolysis products indicates that interconversion of glucose to fructose (by isomerization reaction) did not take place under the studied catalysts and the applied operative conditions. Actually in the literature, glucose isomerization to fructose is reported to occur in the presence of solid strong basic catalysts and/or in the presence of Lewis acidic/Brönsted base pairs [53–55]. The absence of glucose isomerization is then

in accordance with the negligible basicity of CMC-based catalysts, as evidenced by the liquid-solid phase titration results (Fig. S.1.4 and Table S.1.1).

Regarding the catalytic activity of CMC-based materials, exponentially decreasing trends of the sucrose concentration as a function of time-on-stream were observed, in any case. HCMC40 results to be the most performing catalyst, achieving a 50% sucrose conversion in less than 2 h, while pristine CMC and HCMC10 attained the same value after 3.5-4 h.

Kinetic treatment of catalytic data was carried out according to the first order model reaction, as reported in the literature for the sucrose hydrolysis reaction.[46] By plotting *ln [sucrose]* versus *time*, straight lines with high correlation coefficients were obtained for all samples, , thus confirming the assumption of the first order reaction. From the computed regression lines (Fig. 9, b-d-f-h), the observed kinetic constants (k_{obs}) have been obtained for each catalyst and reported in Table 2. It could be noticed that HCMC40 has a k_{obs} value higher than CMC and HCMC10, which approaches that of Amberlite IR-120(H).

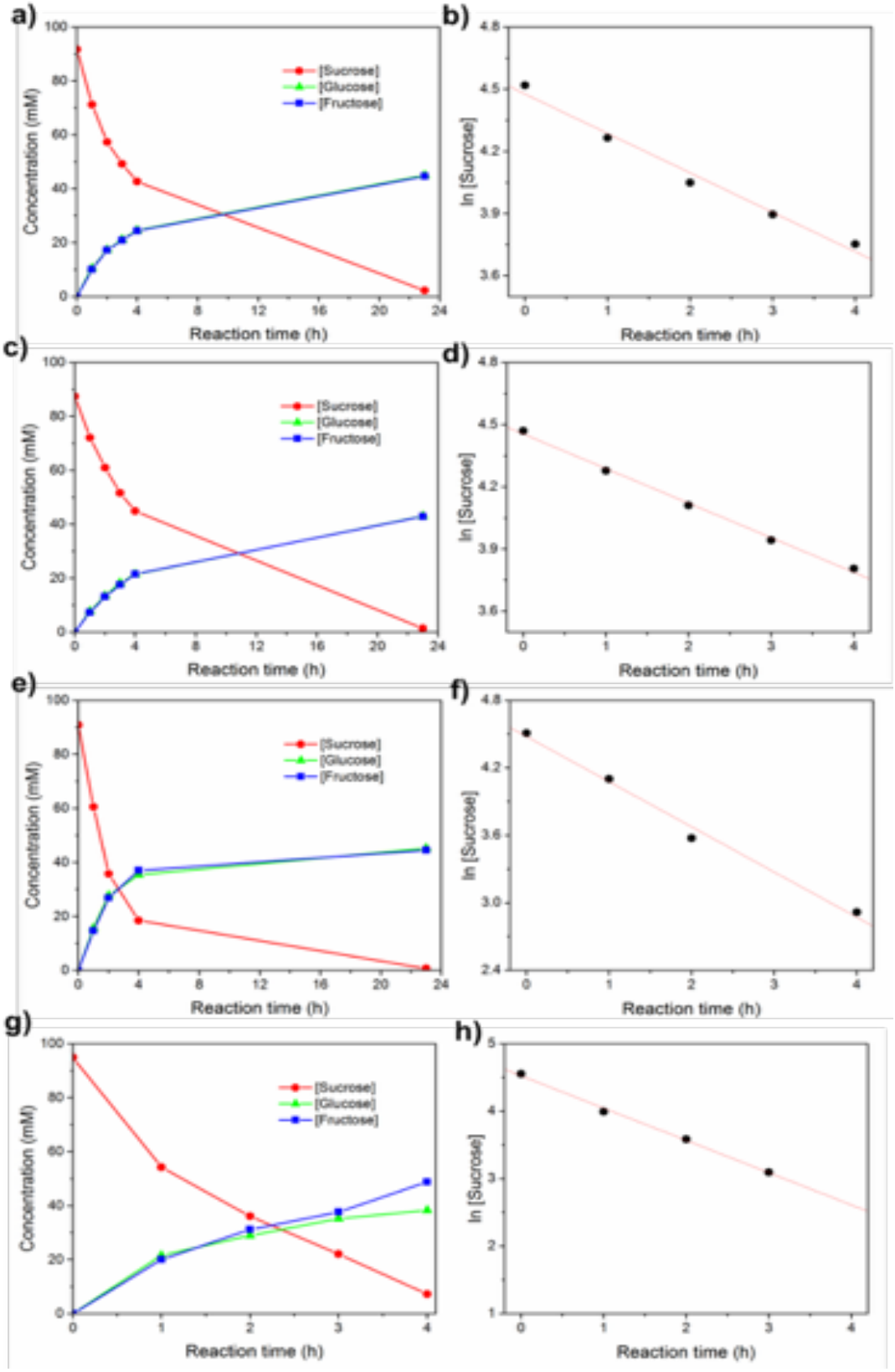

Fig. 9. Concentration profiles of sucrose and formed products (glucose and fructose) as a function of reaction time at 80°C and relevant plots of the linearized *first*-order kinetic equation on CMC (a, b), HCMC10 (c, d), HCMC40 (e, f) and Amberlite (g, h); the slope of the lines correspond to k_{obs} (expressed in h^{-1}).

To have a deeper insight on the reasons responsible of the different observed catalytic behavior, the values of the catalytic constants (k_{cat}) were extrapolated from the k_{obs} values, as described in the Experimental paragraph, considering catalyst concentration expressed in terms of mass (L g^{-1} h^{-1}), or specific surface area (L m^{-2} h^{-1}) or concentration of acidic sites (L mol_{acid}^{-1} h^{-1}).

Table 2. Kinetic (k_{obs}) and catalytic (k_{cat}) constant values of the three carbon-samples in comparison with Amberlite, determined at 80°C in the reaction of hydrolysis of sucrose

Sample	k_{obs} [a] h^{-1}	k_{cat} L g^{-1} h^{-1}	k_{cat} L m^{-2} h^{-1}
Amberlite IR-120(H)	0.478	0.0713	-
CMC	0.190	0.0284	$1.94 \cdot 10^{-5}$
HCMC10	0.166	0.0252	$1.90 \cdot 10^{-5}$
HCMC40	0.401	0.0608	$7.19 \cdot 10^{-5}$

[a] $k_{obs} = k_{cat} \cdot [catalyst]$, with $[catalyst]$ expressed in $g \cdot L^{-1}$, $m^2 \cdot L^{-1}$

As reported in Table 2, when k_{cat} was calculated in L g^{-1} h^{-1} and L m^{-2} h^{-1}, the same trend observed for k_{obs} values and for sucrose conversion could be confirmed. HCMC40 exhibited the higher k_{cat} values among CMC-based samples, approaching that of Amberlite IR-120(H).

4. Conclusions

The most interesting results obtained from this research activity are associated with the tuneable acidity of the samples, in terms of number of acid sites and surface acid strength, obtained from the starting carbon sample (CMC). CMC is a robust material that can be easily functionalized at low temperature without seriously altering the structural-morphological properties.

The carbon samples derived from CMC, after acidic treatment, showed highly acidic surface due to aromatic –COOH and –OH groups, specifically . Strength and density of acid sites in HCMC40

are notable and this marked surface acidity plays a positive role in a catalytic reaction requiring Brönsted acidity (such as sucrose hydrolysis). It is noteworthy that all the three carbons have very good *effective* acidity; that is, acidity is maintained in water. Likely, the surface hydrophobicity of the carbons prevents strong interactions between the acid groups and water, leaving the acid sites available to the reaction , even in the presence of water.

Funding statement

Authors from Università degli Studi di Milano did not receive for this research any specific grant from funding agencies in the public, commercial, or not-for-profit sectors.

Pr. Jianyi Shen acknowledges the financial support from the NSFC (21761132006).

Declaration of Competing Interest

The authors have no financial conflicts of interest to disclose.

Acknowledgements

Authors are indebted with Mr. Fabio Marletta, student of University of Milano, for all his experimental support.

The NMR service of the Technological Platform: "COmprehensive Substances characterization via advanced sPECTtroscopy (COSPECT)", of University of Milano, and in particular Dr. Enrico Caneva are acknowledged for the NMR support.

Analisi & Service of Dipartimento di Chimica, Università degli Studi di Milano, and in particular Dr. Serena Capelli and Mrs. Manuela Gilberti are gratefully thanked for the XPS analyses.

The electron microscopy service of the Technological Platform: "Unitech NOLIMITS" of University of Milano, and in particular Dr. Nadia Santo are acknowledged for the support.

Supplementary information

Paragraph S.1. Pulse liquid phase adsorption experiments for acidity and basicity determination.

Paragraph S.2. NMR characterization of the carbon samples.

Paragraph S.3. Experimental kinetic results of the reaction of catalytic sucrose hydrolysis.

References

1 P. Serp and B. Machado, in *Nanostructured Carbon Materials for Catalysis*, eds. P. Serp and J. L. Figueiredo, John Wiley & Sons, Inc., Hoboken, NJ, USA, 2015, pp. 1–45.

2 F. Rodríguez-reinoso, *Carbon N. Y.*, 1998, **36**, 159–175.

3 X. Liu and L. Dai, *Nat. Rev. Mater.*, 2016, **1**, 16064.

4 A. Thomas, A. Fischer, F. Goettmann, M. Antonietti, J. O. Müller, R. Schlögl and J. M. Carlsson, *J. Mater. Chem.*, 2008, **18**, 4893–4908.

5 D. S. Su, J. Zhang, B. Frank, A. Thomas, X. Wang, J. Paraknowitsch and R. Schlögl, *ChemSusChem*, 2010, 3, 169–180.

6 X. Liu and L. Dai, *Nat. Rev. Mater.*, 2016, **1**, 16064.

7 C. K. Chua and M. Pumera, *Chem. - A Eur. J.*, 2015, **21**, 12550–12562.

8 D. S. Su, S. Perathoner and G. Centi, *Chem. Rev.*, 2013, **113**, 5782–5816.

9 X. SUN, R. WANG and D. SU, *Chinese J. Catal.*, 2013, **34**, 508–523.

10 D. Liu, L. Dai, X. Lin, J. F. Chen, J. Zhang, X. Feng, K. Müllen, X. Zhu and S. Dai, *Adv. Mater.*, 2019, 31, 1–29.

11 L. Dai, *Carbon-Based Metal-Free Catalysts*, Wiley-VCH Verlag GmbH & Co. KGaA, Weinheim, Germany, 2018.

12 W. Qi and D. Su, *ACS Catal.*, 2014, **4**, 3212–3218.

13 F. Atamny, J. Blöcker, A. Dübotzky, H. Kurt, O. Timpe, G. Loose, W. Mahdi and R. Schlögl, *Mol. Phys.*, 1992, **76**, 851–886.

14 J. Luo, H. Yu, H. Wang, H. Wang and F. Peng, *Chem. Eng. J.*, 2014, **240**, 434–442.

15 R. P. Rocha, M. F. R. Pereira and J. L. Figueiredo, *Catal. Today*, 2019.

16 Y. Wang, J. Zhang, X. Wang, M. Antonietti and H. Li, *Angew. Chemie - Int. Ed.*, 2010, **49**, 3356–3359.

17 M. A. Patel, F. Luo, M. R. Khoshi, E. Rabie, Q. Zhang, C. R. Flach, R. Mendelsohn, E. Garfunkel, M. Szostak and H. He, *ACS Nano*, 2016, **10**, 2305–2315.

18 Y. Zheng, Y. Jiao, M. Jaroniec, Y. Jin and S. Z. Qiao, *Small*, 2012, **8**, 3550–3566.

19 J. Zhang, Z. Zhao, Z. Xia and L. Dai, *Nat. Nanotechnol.*, 2015, **10**, 444.

20 Y. Jiao, Y. Zheng, K. Davey and S.-Z. Qiao, *Nat. Energy*, 2016, **1**, 16130.

21 L.-B. Sun, X.-Y. Wei, X.-Q. Liu, Z.-M. Zong, W. Li and J.-H. Kou, *Energy & Fuels*, 2009, **23**, 4877–4882.

22 L. Pacosová, C. Kartusch, P. Kukula and J. A. van Bokhoven, *ChemCatChem*, 2011, **3**, 154–156.

23 Y. Ding, X. Huang, X. Yi, Y. Qiao, X. Sun, A. Zheng and D. S. Su, *Angew. Chemie - Int. Ed.*, 2018, **57**, 13800–13804.

24 M. R. Acocella, M. Mauro and G. Guerra, *ChemSusChem*, 2014, **7**, 3279–3283.

25 F. Hu, M. Patel, F. Luo, C. Flach, R. Mendelsohn, E. Garfunkel, H. He and M. Szostak, *J. Am. Chem. Soc.*, 2015, **137**, 14473–14480.

26 F. Goettmann, A. Fischer, M. Antonietti and A. Thomas, *Angew. Chemie - Int. Ed.*, 2006, **45**, 4467–4471.

27 N. Kausar, P. P. Ghosh, G. Pal and A. R. Das, *RSC Adv.*, 2015, **5**, 60199–60207.

28 S. M. Islam, A. S. Roy, R. C. Dey and S. Paul, *J. Mol. Catal. A Chem.*, 2014, **394**, 66–73.

29 S. Campisi, F. Sanchez Trujillo, D. Motta, T. Davies, N. Dimitratos and A. Villa, *C*, 2018, **4**, 9.

30 P. V Rathod, S. D. Nale and V. H. Jadhav, *ACS Sustain. Chem. Eng.*, 2017, **5**, 701–707.

31 A. Villa, M. Schiavoni, P. F. Fulvio, S. M. Mahurin, S. Dai, R. T. Mayes, G. M. Veith and L. Prati, *J. Energy Chem.*, 2013, **22**, 305–311.

32 E. Lam and J. H. T. Luong, *ACS Catal.*, 2014, **4**, 3393–3410.

33 A. Villa, J. P. Tessonnier, O. Majoulet, D. S. Su and R. Schlögl, 1–2.

34 J. P. Tessonnier, A. Villa, O. Majoulet, D. S. Su and R. Schlögl, *Angew. Chemie - Int. Ed.*, 2009, **48**, 6543–6546.

35 R. Ryoo, S. H. Joo, M. Kruk and M. Jaroniec, *Adv. Mater.*, 2001, **13**, 677–681.

36 X. Jin, V. V. Balasubramanian, S. T. Selvan, D. P. Sawant, M. A. Chari, G. Q. Lu and A. Vinu, *Angew. Chemie - Int. Ed.*, 2009, **48**, 7884–7887.

37 C. M. A. Parlett, K. Wilson and A. F. Lee, *Chem. Soc. Rev.*, 2013, **42**, 3876–3893.

38 H. W. Liang, X. Zhuang, S. Brüller, X. Feng and K. Müllen, *Nat. Commun.*, 2014, **5**, 1–7.

39 D.-W. Wang, F. Li, M. Liu, G. Q. Lu and H.-M. Cheng, *Angew. Chemie Int. Ed.*, 2008, **47**, 373–376.

40 C. Duong-Viet, H. Ba, L. Truong-Phuoc, Y. Liu, J.-P. Tessonnier, J.-M. Nhut, P. Granger and C. Pham-Huu, in *New Materials for Catalytic Applications*, Elsevier, 2016, pp. 273–311.

41 L. J. Konwar, P. Mäki-Arvela and J. P. Mikkola, *Chem. Rev.*, , DOI:10.1021/acs.chemrev.9b00199.

42 A. Sánchez-Sánchez, F. Suárez-García, A. Martínez-Alonso and J. M. D. Tascón, *Carbon N. Y.*, 2013, **62**, 193–203.

43 V. Datsyuk, M. Kalyva, K. Papagelis, J. Parthenios, D. Tasis, A. Siokou, I. Kallitsis and C. Galiotis, *Carbon N. Y.*, 2008, **46**, 833–840.

44 Y. Huang, S. Hu, S. Zuo, Z. Xu, C. Han and J. Shen, *J. Mater. Chem.*, 2009, **19**, 7759–7764.

45 P. Carniti, A. Gervasini and S. Biella, *Adsorpt. Sci. Technol.*, 2005, **23**, 739–749.

46 M. Marzo, A. Gervasini and P. Carniti, *Carbohydr. Res.*, 2012, **347**, 23–31.

47 Z. Q. Li, C. J. Lu, Z. P. Xia, Y. Zhou and Z. Luo, *Carbon N. Y.*, 2007, **45**, 1686–1695.

48 N. Iwashita, in *Materials Science and Engineering of Carbon*, eds. M. Inagaki and F. Kang, Butterworth-Heinemann, 2016, pp. 7–25.

49 Y. Wang, D. C. Alsmeyer and R. L. McCreery, *Chem. Mater.*, 1990, **2**, 557–563.

50 F. Tuinstra and J. L. Koenig, *J. Chem. Phys.*, 1970, **53**, 1126–1130.

51 A. C. Ferrari and J. Robertson, *Phys. Rev. B*, 2000, **61**, 14095–14107.

52 M. V. Lopez-Ramon, F. Stoeckli, C. Moreno-Castilla and F. Carrasco-Marin, *Carbon N. Y.*, 1999, **37**, 1215–1221.

53 V. Choudhary, A. B. Pinar, R. F. Lobo, D. G. Vlachos and S. I. Sandler, *ChemSusChem*, 2013, **6**, 2369–2376.

54 S. S. Chen, D. C. W. Tsang and J.-P. Tessonnier, *Appl. Catal. B Environ.*, 2020, **261**, 118126.

55 S. S. Chen, J. M. Carraher, G. Tuci, A. Rossin, C. A. Raman, L. Luconi, D. C. W. Tsang, G. Giambastiani and J. P. Tessonnier, *ACS Sustain. Chem. Eng.*, 2019, **7**, 16959–16963.

Supplementary information

Tuneable acidity in metal-free mesoporous carbons for hydrolysis reactions

M. Ferri, S. Campisi, P. Carniti, A. Gervasini, J. Shen

Paragraph S.1. Pulse liquid phase adsorption experiments for acidity and basicity determination

To determine surface acidity of the three carbon samples (and also basicity for CMC), a modified HPLC line (Fig. S1) has been used. Solid-liquid acid-base titration with pulse injections of probe molecule (PEA for acidity and BA for basicity) solutions at constant temperature has been performed. The setup allowed determining the surface sample acidity/basicity in different liquids where the probes were dissolved. Titrations performed in non-polar and aprotic liquids (like cyclohexane) allow determining *intrinsic* acidity/basicity, because in this case there are not any interactions between the surface functionalities and the liquid. On the other hand, working in polar and/or protic liquids (like water), surface acid/base centers of the sample can interact with the liquid with, for example, hydrogen bond, or coordinating bond, among other types of interactions. Choosing to determine the acidity/basicity of the sample in the same liquid in which it work (in the present case, reaction of sucrose hydrolysis occurred in water), this allows to measure the *effective* acidity/basicity, which directly correlates with the functional performance (in the present case, catalytic activity).

The mobile phase, in which the probe is dissolved and in which basic/acid probe adsorption is being performed on the sample surface, is withdrawn from a reservoir and, by means of a pump (model L-6200A Merck Hitachi,) it is sent to the sample holder (maintained at constant temperature, typically 30°C±1°C), where the sample to be analyzed was packed. Successively, the mobile phase flows into an UV-Vis detector (model L-4250 Merck Hitachi) that quantifies the probe still present in solution (amount of probe not adsorbed on the sample) to be then, finally, discharged in a collection flask.

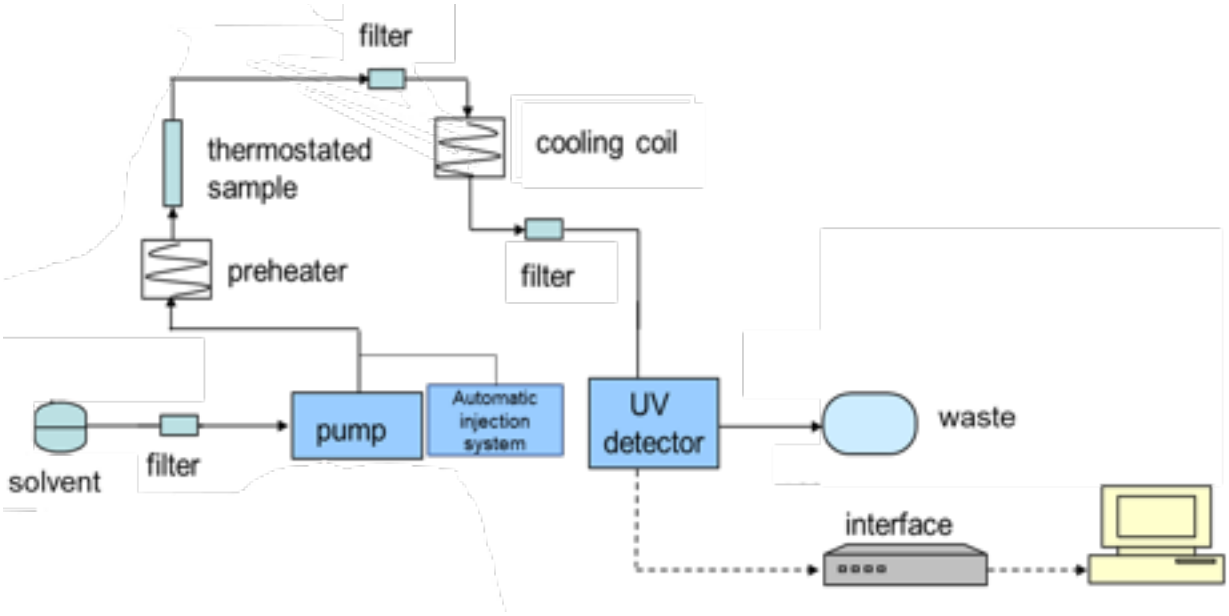

Fig. S.1.1 Scheme of the modified HPLC adsorption line for the collection of pulse liquid-solid titrations of carbon samples in liquid.

Through an automatic sampler (model AS-2000A Merck Hitachi), a small and precise volume (typically from 10 to 50 μL) of the solution of the chosen probe (PEA or BA) in the chosen liquid at known concentration (typically 0.1 M), is injected into the line and flows through the sample. The operation is repeated until saturation of the acid/base sites of the sample surface is attained.

The non-adsorbed probe is revealed by the UV-vis detector as a peak whose area is directly proportional to the quantity of probe, by suitable calibration experiments. The peak area tends to increase with the number of injections, as the quantity of probe adsorbed by the sample tends to diminish. Once saturation is attained, the peak areas have constant value.

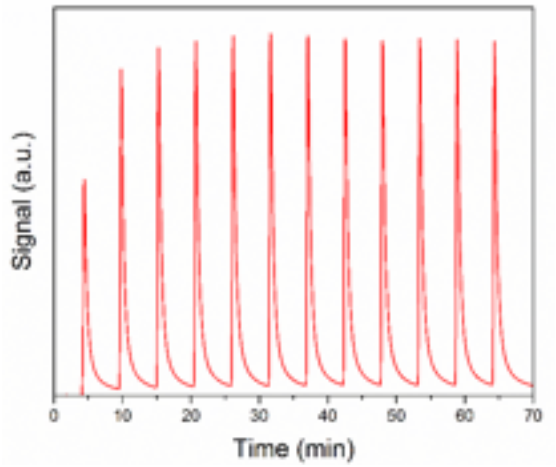

Fig. S.1.2 Example of the obtained chromatogram from pulse liquid phase adsorption experiments.

It is possible to quantify the number of surface acid/base sites by computing the amount of probe adsorbed and assuming a given stoichiometry between the probe and the surface acid/base site:

where:
probe adsorbed (mmol g^{-1}) = quantity of probe molecule adsorbed on the sample during the *i*-injection;
[probe] (mol L^{-1}) = concentration of the injected probe (PEA or BA) solution;
V_{Inj} (mL) = volume of the single *i*-injection;
m_{cat} (g) = mass of sample put in the sample holder;
A_{sat} = average chromatographic area of the peaks at saturation (when constant area value is attained);
A_i = chromatographic area of the *i*-peak.

When a 1:1 stoichiometry between the probe and the site is assumed, the number of acidic/basic sites of the analyzed sample corresponds to the total amount of probe molecule adsorbed:

It is then possible to express the total number of surface acid/base sites of the sample as mequiv. g^{-1} or μequiv. m^{-2}.

Fig. S.1.3 Scheme of the NH_3-TPD experimental set-up and typical output.

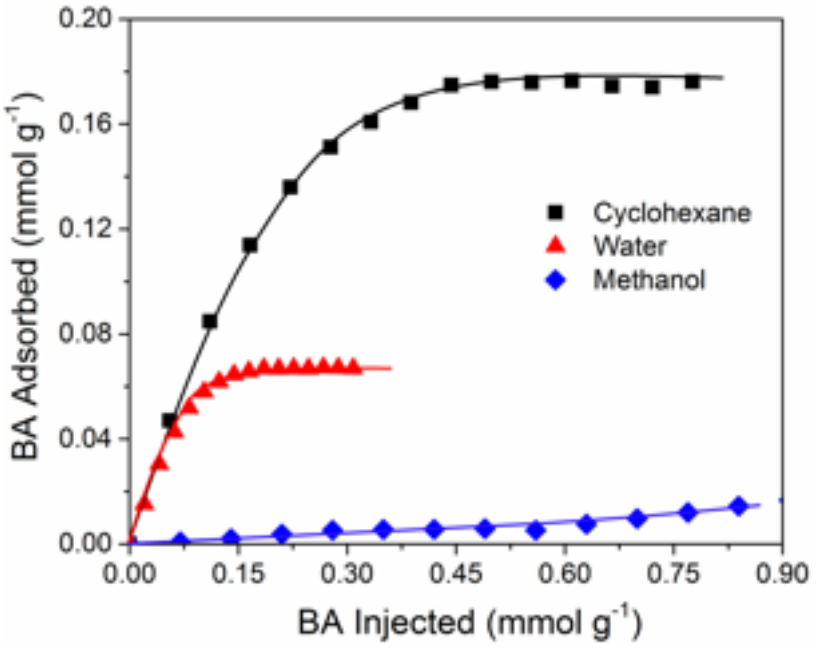

Fig. S.1.4 Results of the CMC basicity obtained from the pulse liquid phase adsorption experiments with BA in three different solvents: cyclohexane, water; and methanol (BA was monitored at λ = 254 nm) Titrations have been performed under the same conditions described for the surface acidity measurements in the experimental section.

Table S.1. Results of acidity and basicity titrations determined with PEA and BA probes, respectively by pulse liquid phase adsorption experiments in different solvents (T = 25 ± 2°C).

Sample	**Acidity**					
	cyclohexane		water		methanol	
	mequiv. g^{-1}	μequiv m^{-2}	mequiv. g^{-1}	μequiv. m^{-2}	mequiv. g^{-1}	μequiv. m^{-2}
CMC	0.499	0.341	0.484	0.330	0.173	0.118
HCMC10	0.843	0.633	0.839	0.630	0.263	0.198
HCMC40	1.182	1.399	1.118	1.323	0.248	0.294
Amberlite IR-120(H)[a]	-	-	2.270	-	-	-

Sample	**Basicity**					
	cyclohexane		water		methanol	
	mequiv. g^{-1}	μequiv. m^{-2}	mequiv. g^{-1}	μequiv. m^{-2}	mequiv. g^{-1}	μequiv. m^{-2}

CMC	0.175	0.120	0.0669	0.0457	0.0501	0.0342

[a] Data from reference [45]

As shown in Fig. S3 and reported in Tab S1, CMC exhibits a limited number of surface basic sites. The trend of the basic site accessibility *vs.* nature of solvent is the same of that has been found for acidity.

Basicity of the HCMC10 and HCMC40 samples has not been determined as the acidic functionalization performed on CMC for the sample preparation has suppressed any basicity.

Paragraph S.2. NMR characterization of the carbon samples

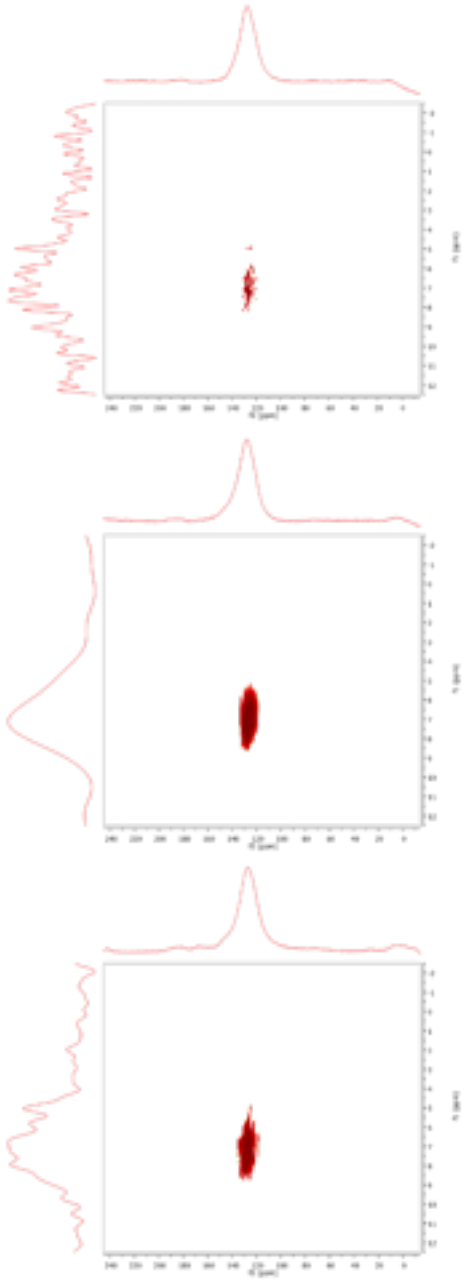

Figure S.2. ^{1}H-^{13}C 2D dipolar coupling NMR spectra of a) CMC; b) HCMC10; c) HCMC40.

Paragraph S.3. Experimental kinetic results of the reaction of catalytic sucrose hydrolysis

Tables S2-S5 report all the data and results collected during the catalytic tests of sucrose hydrolysis performed on the Amberlite IR-120(H), CMC, HCMC10, and HCMC40 samples. As reported in the experimental section, sucrose hydrolysis reaction has been performed in aqueous solution ($V_{solution}$ = 150 mL, [Sucrose] ≈ 100 mM) at 80°C, and under vigorous stirring (400 RPM). Catalyst to solution volume ratio has been kept constant at *ca.* 0.0067 g mL^{-1}.

Table S.3.1 Results of catalytic hydrolysis of sucrose on Amberlite

Reaction time	Concentration				Conversion	Selectivity		Yield	
	Sucrose	Glucose	Fructose	Total	Sucrose	Glucose	Fructose	Glucose	Fructose
(h)	(meq. monosaccharides L^{-1})				(%)	(%)		(%)	
0	94.89	0	0	94.89	0	0	0	0	0
1	54.27	21.56	20.08	95.91	42.81	53.08	49.43	22.72	21.16
2	36.12	28.97	31.17	96.26	61.93	49.29	53.04	30.53	32.85
3	22.1	35.26	37.66	95.02	76.71	48.44	51.74	37.16	39.69
4	7.28	38.30	48.77	94.35	92.33	43.71	55.67	40.36	51.40

Table S.3.2 Results of catalytic conversion of sucrose on CMC

Reaction time	Concentration				Conversion	Selectivity		Yield	
	Sucrose	Glucose	Fructose	Total	Sucrose	Glucose	Fructose	Glucose	Fructose
(h)	(meq. monosaccharides L^{-1})				(%)				
0	91.71	0	0	91.71	0	0	0	0	0
1	71.23	10.55	10.06	91.84	22.33	51.51	49.12	11.50	10.97
2	57.34	17.36	17.18	91.88	37.48	50.51	49.99	18.93	18.73
3	49.24	21.1	20.88	91.22	46.31	49.68	49.16	23.01	22.77
4	42.65	24.66	24.4	91.71	53.49	50.26	49.74	26.89	26.61
ca. 23	2.24	45.01	44.65	91.90	97.56	50.31	49.90	49.08	48.69

Table S.3.3 Results of catalytic conversion of sucrose on HCMC10

Reaction time	Concentration				Conversion	Selectivity		Yield	
	Sucrose	Glucose	Fructose	Total	Sucrose	Glucose	Fructose	Glucose	Fructose

(h)	(meq. monosaccharides L^{-1})				(%)				
0	87.44	0	0	87.44	0	0	0	0	0
1	72.12	7.75	7.3	87.17	17.52	50.59	47.65	8.86	8.35
2	61.04	13.49	13.09	87.62	30.19	51.10	49.58	15.43	14.97
3	51.6	18.25	17.59	87.44	40.99	50.92	49.08	20.87	20.12
4	44.96	21.5	21.55	88.01	48.58	50.61	50.73	24.59	24.65
ca. 23	1.37	43.05	42.87	87.29	98.43	50.02	49.81	49.23	49.03

Table S.3.4 Results of catalytic conversion of sucrose on HCMC40

Reaction time	Concentration				Conversion	Selectivity		Yield	
	Sucrose	Glucose	Fructose	Total	Sucrose	Glucose	Fructose	Glucose	Fructose
(h)	(meq. monosaccharides L^{-1})				(%)				
0	90.82	0	0	90.82	0	0	0	0	0
1	60.5	15.63	14.65	90.78	33.38	51.55	48.32	17.21	16.13
2	35.75	27.74	26.8	90.29	60.64	50.37	48.67	30.54	29.51
4	18.48	35.39	37.04	90.91	79.65	48.92	51.20	38.97	40.78
ca. 23	0.71	45.19	44.48	90.38	99.22	50.15	49.36	49.76	48.98